Experimental investigation on Brillouin scattering property in highly nonlinear photonic crystal fiber with hybrid core

Weiwen Zou,[1,2,3] Zuyuan He,[1,4] and Kazuo Hotate[1,5]

[1]*Department of Electrical Engineering and Information Systems, The University of Tokyo, Tokyo 113-8656, Japan*
[2]*State Key Laboratory of Advanced Optical Communication Systems and Networks, Department of Electronic Engineering, Shanghai Jiao Tong University, Shanghai 200240, China*
[3]*wzou@sjtu.edu.cn*
[4]*zhe@ieee.org*
[5]*hotate@sagnac.t.u-tokyo.ac.jp*

Abstract: Brillouin scattering property in a highly nonlinear photonic crystal fiber (HNL-PCF) with hybrid-core structure is experimentally investigated. The HNL-PCF comprises a highly Ge-doped core surrounded by a triangularly-arranged F-doped buffer. It is experimentally shown that there exist five Brillouin resonance peaks with ~300 MHz frequency spacing in the Brillouin gain spectrum, which can be classified into two groups physcially attributed to two spatially separated layers of Ge-doped and F-doped regions. These peaks have similar linear dispersion characteristics and their effective acoustic velocities increase monotonically by the order of the peaks. The acousto-optic overlapping efficiency in the fiber is measured to be ~50%, which indicates that the stimulated Brillouin scattering threshold in the HNL-PCF is twofold enhanced. The temperature and strain dependences of the first resonance peak are also investigated, showing the similar behaviors as those in all-silica optical fibers.

OCIS codes: (290.5900) Scattering, stimulated Brillouin; (120.5820) Scattering measurements; (060.5295) Photonic crystal fibers; (060.2270) Fiber characterization.

References and links

1. J. C. Knight, "Photonic crystal fibres," Nature **424**(6950), 847–851 (2003).
2. K. Chow, C. Shu, C. Lin, and A. Bjarklev, "Polarization-insensitive widely tunable wavelength converter based on four-wave mixing in a dispersion-flattened nonlinear photonic crystal fiber," IEEE Photon. Technol. Lett. **17**(3), 624–626 (2005).
3. J. Dudley, G. Genty, and S. Coen, "Supercontinuum generation in photonic crystal fiber," Rev. Mod. Phys. **78**(4), 1135–1184 (2006).
4. L. Zou, X. Bao, and L. Chen, "Brillouin scattering spectrum in photonic crystal fiber with a partially germanium-doped core," Opt. Lett. **28**(21), 2022–2024 (2003).
5. A. Yeniay, J. M. Delavaux, and J. Toulouse, "Spontaneous and stimulated Brillouin scattering gain spectra in optical fibers," J. Lightwave Technol. **20**(8), 1425–1432 (2002).
6. Y. Koyamada, S. Sato, S. Nakamura, H. Sotobayashi, and W. Chujo, "Simulating and designing Brillouin gain spectrum in single-mode fibers," J. Lightwave Technol. **22**(2), 631–639 (2004).
7. W. Zou, Z. He, M. Kishi, and K. Hotate, "Stimulated Brillouin scattering and its dependences on strain and temperature in a high-delta optical fiber with F-doped depressed inner cladding," Opt. Lett. **32**(6), 600–602 (2007).
8. P. Dainese, P. St. J. Russell, N. Joly, J. C. Knight, G. S. Wiederhecker, H. L. Fragnito, V. Laude, and A. Khelif, "Stimulated Brillouin scattering from multi-GHz-guided acoustic phonons in nanostructured photonic crystal fibers," Nat. Phys. **2**(6), 388–392 (2006).
9. P. Dainese, P. St. J. Russell, G. S. Wiederhecker, N. Joly, H. L. Fragnito, V. Laude, and A. Khelif, "Raman-like light scattering from acoustic phonons in photonic crystal fiber," Opt. Express **14**(9), 4141–4150 (2006).
10. A. Kobyakov, S. Kumar, D. Q. Chowdhury, A. B. Ruffin, M. Sauer, S. R. Bickham, and R. Mishra, "Design concept for optical fibers with enhanced SBS threshold," Opt. Express **13**(14), 5338–5346 (2005).
11. W. Zou, Z. He, and K. Hotate, "Experimental study of Brillouin scattering in fluorine-doped single-mode optical fibers," Opt. Express **16**(23), 18804–18812 (2008).

#160578 - $15.00 USD Received 3 Jan 2012; revised 2 Mar 2012; accepted 31 Mar 2012; published 30 Apr 2012

12. T. Horiguchi, T. Kurashima, and M. Tateda, "Tensile strain dependence of Brillouin frequency shift in silica optical fibers," IEEE Photon. Technol. Lett. **1**(5), 107–108 (1989).
13. W. Zou, Z. He, and K. Hotate, "Investigation of strain- and temperature-dependences of Brillouin frequency shifts in GeO_2-doped optical fibers," J. Lightwave Technol. **26**(13), 1854–1861 (2008).
14. J. E. McElhenny, R. K. Pattnaik, J. Toulouse, K. Saitoh, and M. Koshiba; "Unique characteristic features of stimulated Brillouin scattering in small-core photonic crystal fibers," J. Opt. Soc. Am. B **25**(4), 582–593 (2008).
15. W. Zhang, Y. Wang, Y. Pi, Y. Huang, and J. Peng, "Influences of pump wavelength and environment temperature on the dual-peaked Brillouin property of a small-core microstructure fiber," Opt. Lett. **32**(16), 2303–2305 (2007).
16. W. Zou, Z. He, and K. Hotate, "Complete discrimination of strain and temperature using Brillouin frequency shift and birefringence in a polarization-maintaining fiber," Opt. Express **17**(3), 1248–1255 (2009).
17. W. Zou, Z. He, K.-Y. Song, and K. Hotate, "Correlation-based distributed measurement of a dynamic grating spectrum generated in stimulated Brillouin scattering in a polarization-maintaining optical fiber," Opt. Lett. **34**(7), 1126–1128 (2009).
18. W. Zou, Z. He, and K. Hotate, "Demonstration of Brillouin distributed discrimination of strain and temperature using a polarization-maintaining optical fiber," IEEE Photon. Technol. Lett. **22**(8), 526–528 (2010).
19. W. Zou, Z. He, and K. Hotate, "One-laser-based generation/detection of Brillouin dynamic grating and its application to distributed discrimination of strain and temperature," Opt. Express **19**(3), 2363–2370 (2011).
20. K. Hotate and T. Hasegawa, "Measurement of Brillouin gain spectrum distribution along an optical fiber using a correlation-based technique — Proposal, experiment and simulation," IEICE Trans. Electron, E **83-C**, 405–412 (2000).
21. K.-Y. Song, Z. He, and K. Hotate, "Distributed strain measurement with millimeter-order spatial resolution based on Brillouin optical correlation domain analysis," Opt. Lett. **31**(17), 2526–2528 (2006).
22. K. Hansen, "Dispersion flattened hybrid-core nonlinear photonic crystal fiber," Opt. Express **11**(13), 1503–1509 (2003).
23. W. Zou, Z. He, and K. Hotate, "Acoustic modal analysis and control in *w*-shaped triple-layer optical fibers with highly-germanium-doped core and F-doped inner cladding," Opt. Express **16**(14), 10006–10017 (2008).
24. W. Zou, Z. He, and K. Hotate, "Two-dimensional finite element modal analysis of Brillouin gain spectra in optical fibers," IEEE Photon. Technol. Lett. **18**(23), 2487–2489 (2006).

1. Introduction

Photonic crystal fibers (PCFs) have been widely studied during last decades because they show great potential in both telecommunication applications [1–3] and non-communication fields, such as Brillouin-based fiber-optic distributed sensing systems [4]. Both applications need the knowledge of Brillouin scattering property in the PCF, including the Brillouin resonance peaks [5–9], the acousto-optic overlapping efficiency [10, 11], and the dependence on strain and temperature [12, 13]. So far, it has been reported that the confinement of optical and acoustic waves in an air-silica photonic crystal fiber (PCF) is diversely dependent on the PCF structure [4, 8, 9, 14, 15], and different from that in an all-silica optical fiber [5–7], which results in different Brillouin scattering property in PCFs. The threshold of stimulated Brillouin scattering (SBS) in a small-core PCF was reported to be fivefold enhanced with multiple discrete resonance peaks in the Brillouin gain spectrum (BGS) [8]; while multiple-peak BGS was also observed in small-core all-silica optical fibers [5–7]. McElhenny *et al.* reported that the acoustic dispersion characteristics of the resonance peaks in small-core PCFs are dependent to the order of the peaks [14], while Zhang *et al.* reported that the acoustic dispersion characteristics are not linear [15]. These dispersion characteristics are quite unique as compared to those in all-silica optical fibers [5–7, 11]. The physical reasons were possibly attributed to the existence of phononic bandgap [9], or to the fact that the longitudinal acoustic modes are coupled with the shear acoustic modes in the core region of the PCFs via the air-silica microstructure [8, 14, 15]. The fact was also thought to be the physical reason why the dependences of multiple resonance peaks on strain and temperature are different [4], which was expected to be useful for the discriminative sensing of strain and temperature in Brillouin-based distributed sensors, although the performance of discrimination is quite poorer than the new proposal based on polarization maintaining all-silica fibers [16–19].

In this paper, we present an experimental investigation on the SBS property in a highly nonlinear photonic crystal fiber (HNL-PCF) with a hybrid core of highly Ge-doped and F-doped regions. It was experimentally observed five Brillouin resonance peaks with ~300 MHz frequency spacing in the BGS. All the resonance peaks show similar linear dispersion

#160578 - $15.00 USD Received 3 Jan 2012; revised 2 Mar 2012; accepted 31 Mar 2012; published 30 Apr 2012

characteristics and have monotonically increasing effective acoustic velocities by the order of the peaks. The resonance peaks in the HNL-PCF can be divided into two groups according to the measured BGS profile and the deduced effective acoustic velocities. These two groups are physically attributed to two spatially separated layers of Ge-doped and F-doped regions at the hybrid core. Additionally, we found that the acousto-optic overlapping efficiency in the HNL-PCF is halved, showing the twofold enhancement of the SBS threshold. It is also studied the temperature and strain dependences of the first resonance peak in the HNL-PCF. The investigated results of the SBS property including the two spatially separated groups and the monotonically incremental dispersion characteristics in the HNL-PCF are quite similar with all-silica optical fibers [11, 13] but different from the previous observations in other types of PCF [8, 9, 14, 15]. The strain and temperature dependences do not show significant feasibility for discriminative sensing of strain and temperature as observed in [4].

2. Experiments

The experimental setup to measure the SBS property is based on the pump-probe scheme as depicted in Fig. 1, which was partially demonstrated in [11]. The light source of the setup is a tunable laser (tunable range 1532~1565 nm) or a distributed feedback laser diode (DFB-LD) (1550 nm). The tunable laser is used to investigate the SBS property in the entire-length of the fiber under test as shown in [11]; while the DFB-LD is employed to study the SBS distribution along the fiber based on Brillouin optical correlation-domain analysis (BOCDA) technique [20, 21]. The lightwave from the light source is divided into two beams via a 3-dB coupler. One beam serving as the SBS pump wave is chopped for lock-in detection, and is amplified by a tunable high-power erbium-doped fiber amplifier (EDFA). The other beam is serving as the SBS probe wave, which frequency is down-shifted to around the Brillouin frequency shift of the HNL-PCF by a single-sideband modulator (SSBM), and is amplified by another EDFA. The Brillouin-amplified probe wave is detected by a photo-detector (PD) and demodulated by a lock-in amplifier (LIA). An optical spectrum analyzer (OSA) is used to characterize the Brillouin gain dependence on the pump power so as to study the acousto-optic overlapping efficiency. Note that two adaptors ("a" and "b") are illustrated in Fig. 1 to denote the locations of changing the laser sources and the characterization devices, respectively.

The hybrid-core HNL-PCF (Crystal Fiber A/S, NL-1550-NEG-1) that we studied comprises a highly GeO_2-doped core (n_1 = ~1.487) surrounded by a triangularly-arranged F-doped buffer (n_2 = ~1.440) [22], which is different from those reported in [8, 9, 14, 15]. The cross section is shown in the inset of Fig. 2. The core diameter is ~2.1 μm and the mode field diameter is ~2.8 μm. The effective refractive index (n_{eff} = 1.457) and the optical effective area (A_{eff} = 6.2 μm^2) are estimated approximately. The HNL-PCF (~9 m) was home-spliced to standard SMF pigtails (~15 cm at each end) through ~5-cm high-delta fibers (HDFs) for mode-field matching. The HDF has a core radius of 1.5 μm, a numerical aperture (NA) of NA = 0.266, optical loss of 1.02 dB/km, and a cutoff frequency of 1.043 μm [13]. It is noted that the BGS of the HDF [13] sits close to that of the HNL-PCF sample that will be demonstrated below, therefore the length of two HDF segments (~10 cm) is cut as short as possible and far shorter than the HNL-PCF sample (~9 m) in order to avoid its influence to the HNL-PCF. The entire loss including the splicing loss and the transmission loss (~9 dB/km for the HNL-PCF) is ~4 dB.

#160578 - $15.00 USD Received 3 Jan 2012; revised 2 Mar 2012; accepted 31 Mar 2012; published 30 Apr 2012

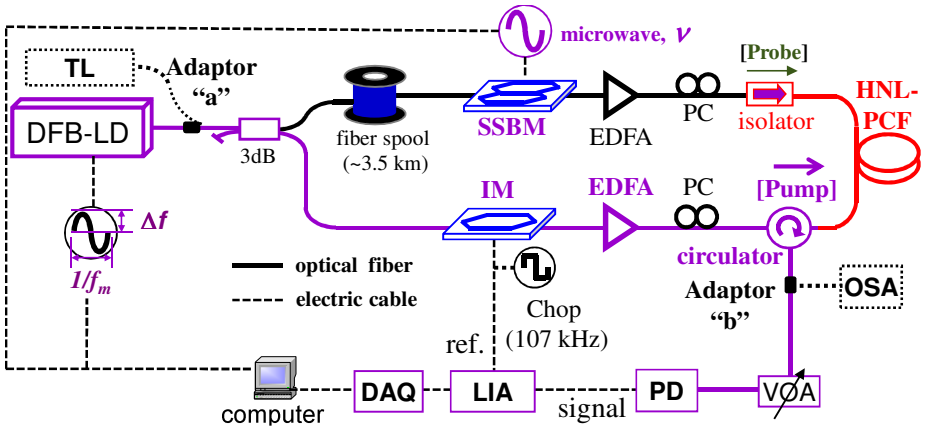

Fig. 1. Experimental setup for characterizing Brillouin scattering property in the HNL-PCF. A tunable laser (TL) of 1532-1565 nm is used for entire measurement. A distributed feedback laser diode (DFB-LD) at 1550 nm under sinusoidal frequency modulation is used for distributed measurement. SSBM: single sideband modulator; EDFA: erbium-doped fiber amplifier; IM: intensity modulator; PC: polarization controller; VOA: variable optical attenuator; PD: photo detector; LIA: lock-in amplifier; DAQ: data acquisition card.

The BGS measured at 1550 nm (with tunable laser source) is illustrated in Fig. 2 that exhibits five discrete resonance peaks. It is noted that the probe power is ~7 dBm and the pump power is ~21 dBm. The resonance frequency spacing between neighboring peaks is about 300 MHz, which is quite similar to highly Ge-doped all-silica fibers [5–7,11,23]. This is possibly due to the high NA and the small core radius of the HNL-PCF sample [23]. Generally, the resonance frequencies (ν_i) of the BGS in an optical fiber are given by

$$\nu_i = 2n_{eff} V_a^i / \lambda, \qquad (1)$$

where V_a^i is the effective acoustic velocity of the i-th order acoustic modes and λ the laser wavelength.

Five-peak Lorentz fitting to the experimental result (see Fig. 2) provides the parameters of each SBS resonance peak, including the Brillouin resonance frequency (ν_i), the Brillouin linewidth ($\Delta\nu_i$), and the relative amplification of each resonance to the first peak (g_i/g_1) in unit of dB, which are summarized in Table 1. The first and the third peaks have narrower Brillouin linewidth and greater Brillouin amplification than the second, the forth and the fifth peaks, which shows that the five peaks can be classified into two separated groups and the first peak and the third peak are their dominant resonance modes. The two separated groups are due to the existence of two kinds of acoustic waveguides in the HNL-PCF. The first kind is formed between the Ge-doped core and the F-doped buffer plus the air-silica microstructured cladding, and the second kind is formed between the F-doped buffer and the microstructured cladding. This situation is quite similar to the all-silica optical fibers [5,23], but the effect of the air-silica microstructure, i.e., the phononic bandgap [9] or the longitudinal-shear overlapping [8,14,15], does not work significantly.

As we have theoretically demonstrated in [23], a great contrast of refractive index (dopant concentration) between the Ge-doped core and the F-doped buffer results in a better confinement of optical mode as well as the lower-order acoustic modes. Besides, the critical condition whether the higher-order acoustic mode enters the F-doped buffer is also sensitive to the core size of the Ge-doped core as well as the normalized v value [23]. Since the radius of the Ge-doped core in the HNL-PCF is as small as ~1.05 μm, it is reasonable to understand that the higher-order (such as above the third-order in this fiber) acoustic modes locate in the F-doped buffer, which principally explains the existence of the two separated two groups of

#160578 - $15.00 USD Received 3 Jan 2012; revised 2 Mar 2012; accepted 31 Mar 2012; published 30 Apr 2012

the Brillouin resonance peaks. However, there is still a difference between the HNL-PCF and the highly-doped all-silica fiber [5, 23], that is, the frequency spacing in the second group is comparable to (denser than) that in the first group in the HNL-PCF (highly-doped all-silica fiber). It is possibly because the air-silica microstructured cladding surrounding the F-doped region generates the phononic bandgap or induces the shear acoustic modes overlapping with the longitudinal acoustic modes [8, 14, 15]. The quantitative explanation of the overall experimental results needs a detailed theoretical and numerical analysis of the BGS in the HNL-PCF by use of two-dimensional finite element method [24], which is under next-plan study.

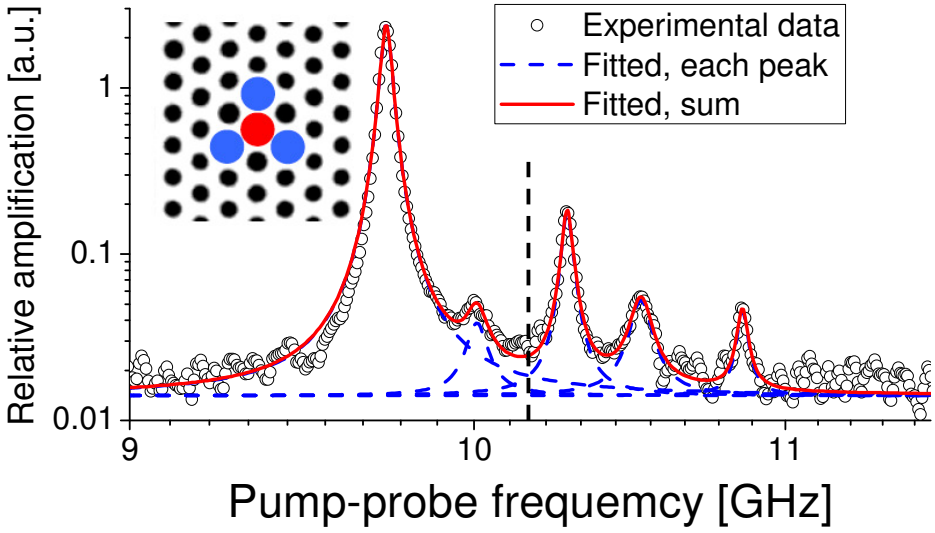

Fig. 2. BGS of the HNL-PCF measured at 1550 nm. The inset shows the fiber's cross section. The dashed line distinguishes the two groups of Brillouin resonance peaks.

Table 1. Summary of Measured and Deduced Parameters of all SBS Resonance Peaks of the HNL-PCF at 1550nm

	Peak 1	**Peak 2**	**Peak 3**	**Peak 4**	**Peak 5**
ν_i (GHz)	9.735	10.009	10.290	10.524	10.856
$\Delta\nu_i$(MHz)	38	71	40	77	40
g_i/g_1 (dB)	0	–22	–12	–17	–21
k_i ($\times 10^4$ m/s)	1.51	1.55	1.60	1.63	1.68
V_a^i (m/s)	5181	5318	5490	5593	5765

By tuning the wavelength λ of the tunable laser, we repeat the BGS measurement and the evaluation of all five resonance frequencies ν_i. Figure 3 summarizes the dispersion characteristics of all five resonance peaks, i.e. ν_i as a function of optical wave number λ^{-1}. All the peaks show good linear-dependence. The dependence slope (k_i) is defined by [10]

$$k_i = \frac{\partial \nu_i}{\partial \lambda^{-1}} = 2n_{eff} V_a^i, \tag{2}$$

which can be deduced by the least-squares linear fitting to the characterized dispersion property (see Fig. 3). Considering the estimated effective refractive index (n_{eff} = 1.457), the

#160578 - $15.00 USD Received 3 Jan 2012; revised 2 Mar 2012; accepted 31 Mar 2012; published 30 Apr 2012

effective acoustic velocities (V_a^i) of all five resonance peaks are deduced. The results are summarized in Table 1. It shows that five resonance peaks have monotonically increasing effective acoustic velocities by the order of the peaks. According to the refractive indices of the hybrid-core HNL-PCF, the acoustic velocities in Ge-doped or F-doped regions are calculated to be 4976 m/s or 5340 m/s [6, 21], respectively. Since the effective acoustic velocities of the first and second peaks are below while those of the third, fourth and fifth peaks are beyond the acoustic velocity of the F-doped region, it can be further ascertained that the first and the second resonance peaks are due to the first-kind acoustic waveguide, while the third, the fourth, and the fifth resonance peaks come from the second-kind acoustic waveguide. It is worth noting that the dispersion characteristics of all resonance peaks SBS is similar to those in all-silica optical fibers [5–7, 11], but different from the results reported in other types of PCFs [14, 15]. It is possibly again due to the tight confinement of all acoustic modes in the all-silica (Ge-doped or F-doped) regions of the HNL-PCF.

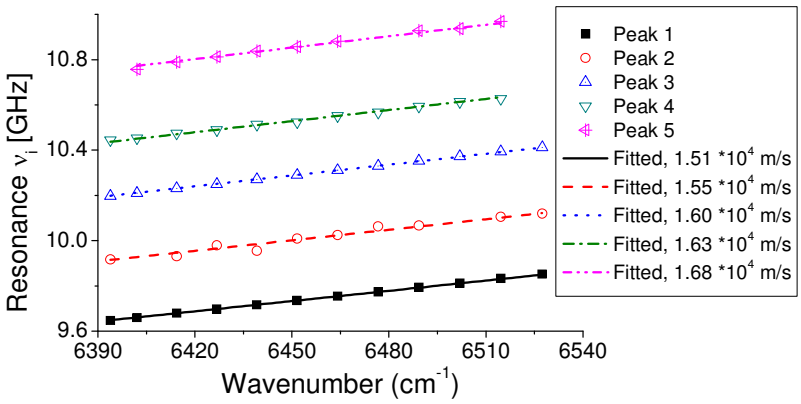

Fig. 3. Acoustic dispersion characteristics of the Brillouin resonance peaks of the HNL-PCF.

To evaluate the acousto-optic overlapping efficiency in the HNL-PCF, as depicted in Fig. 1, we used an optical spectrum analyzer (Advantest Q8384 with 0.02 nm spectral resolution and 0.05 dB power accuracy) to measure the spectra of the probe wave at 1550 nm when the pump wave is turned off or on. An example of the measured spectra is plotted in Fig. 4(a). The SSBM is driven at 9.735 GHz of the first-peak ν_1 and the probe power is reduced to –30 dBm when the EDFA in this arm is removed. The Brillouin amplification gain (G, in dB) is evaluated between on and off states of the pump wave that is set at different optical power (P_p). The result is illustrated in Fig. 4(b). The Brillouin amplification rate (η, in mW^{-1}) is defined by [11]

$$\eta = \frac{\partial G}{\partial P_p} = \frac{\kappa}{K} \cdot g_0 \cdot L_{eff} \,/\, A_{eff}^{\,ao}, \tag{3}$$

where $g_0 = 1.7 \times 10^{-11}$ m/W is the Brillouin gain coefficient [10], $L_{\text{eff}} = 8.9$ m the effective length, $\kappa = 4.343$, and $A_{\text{eff}}^{\text{ao}}$ the effective acousto-optic area [9]. The polarization factor ($1 \le K \le 2$) is dependent on the pump and probe waves' polarization states, that is, $K = 2$ for a complete polarization scrambling process [11] while $K = 1$ for identical polarizations in this study. As shown in Fig. 4(b), we obtained $\eta = 0.053$ mW^{-1} by the linear fitting with the standard error of 0.2%, and deduce the effective acousto-optic area $A_{eff}^{ao} = 12.4$ μm^2. Considering the optical effective area $A_{\text{eff}} = 6.2$ μm^2, the SBS acousto-optic overlapping efficiency [10] is calculated to be $A_{eff}/A_{eff}^{ao} = \sim 50\%$, which means that the SBS threshold is twofold enhanced. Compared to the SBS threshold obtained simply by measuring the reflection power [8], our measurement provides higher accuracy. This is because we fully eliminated the influence to the measured Brillouin amplification gain (G) of the

#160578 - $15.00 USD Received 3 Jan 2012; revised 2 Mar 2012; accepted 31 Mar 2012; published 30 Apr 2012

reflected/backscattered pump wave [see Fig. 4(a)] from the fiber splicing and the Rayleigh scattering.

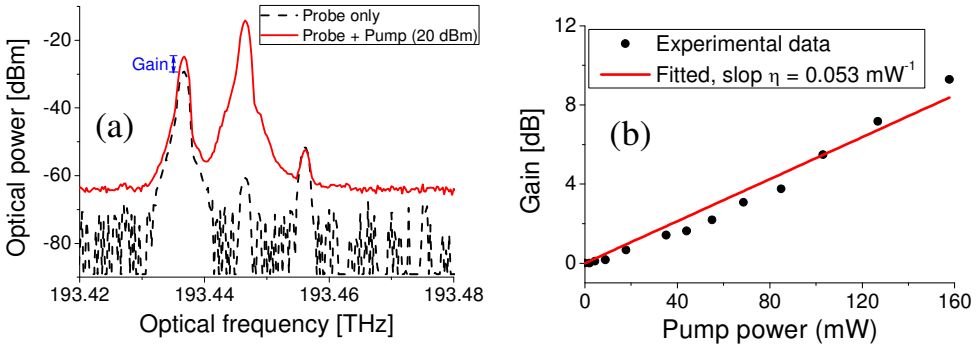

Fig. 4. (a) Example of measured optical spectra with pump wave on (solid) and off (dashed) when the probe power is –30 dBm. (b) Brillouin gain of the first peak as a function of pump power. Dots denote the experimental data and the solid curve corresponds to the least-squares linear fitting.

To study the distributed SBS along the HNL-PCF, the DFB-LD under a sinusoidal frequency modulation was employed as the laser source instead. The modulation frequency is ~6.5 MHz and the modulation depth is 1.2 GHz. The measurement range and the nominal spatial resolution of the distributed measurement are correspondingly ~18 m and ~15 cm, respectively [20]. The distribution of the first-peak resonance frequency ν_1 (i.e. Brillouin frequency shift) along the HNL-PCF was characterized as plotted in Fig. 5(a). The HNL-PCF was hand-wounded to eliminate any residual bending strain/stress in the fiber spool. It is confirmed by repeatability test that the ν_1 fluctuates within a range of 15 MHz along the HNL-PCF length, which is possibly attributed to the longitudinal residual strain/stress stored into the HNL-PCF during the fiber fabrication.

We applied different temperature changes to a ~25-cm-long segment (A) at the position of ~1.4 m, and different static strains to a ~20-cm-long segment (B) at the position of ~2.1 m several times. The distributed SBS around the two segments were repeatedly measured and the measured examples are illustrated in Fig. 5(b). The measured temperature and strain dependence are plotted in Figs. 6(a) and 6(b), respectively. By use of the linear fitting to the experimental results, the temperature and strain coefficients are estimated to be 0.99 MHz/°C and 0.038 MHz/με, which are close to those in all-silica optical fibers [11, 13, 16].

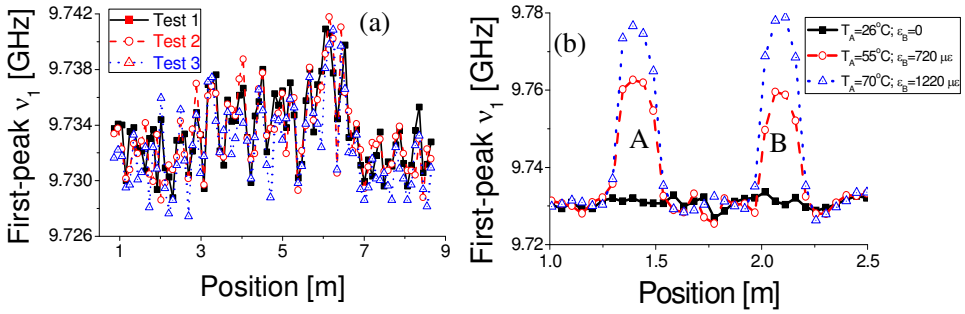

Fig. 5. (a) The distribution of the first-peak resonance frequency ν_1 along the ~9-m HNL-PCF. (b) The ν_1 distribution around the heated and strained fiber segments.

#160578 - $15.00 USD Received 3 Jan 2012; revised 2 Mar 2012; accepted 31 Mar 2012; published 30 Apr 2012

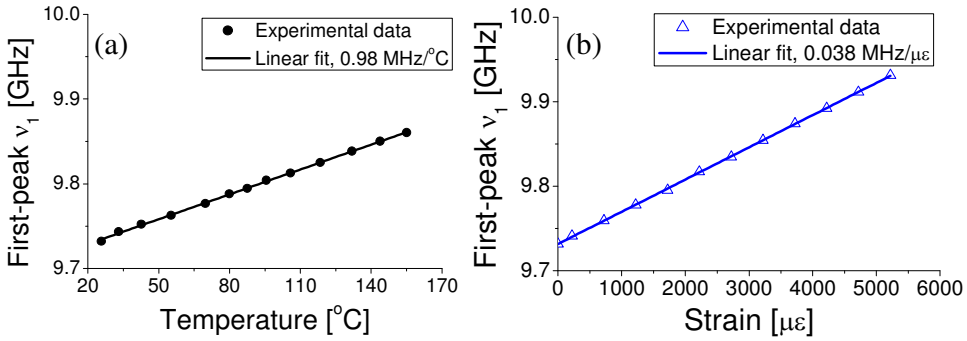

Fig. 6. (a) Temperature and (b) strain dependence of the first-peak resonance frequency of the HNL-PCF.

3. Conclusion

We have investigated the SBS property in the HNL-PCF. Due to the F-doped buffer in the hybrid-core structure, the BGS exhibits five resonance peaks classified into two groups. All five resonance peaks have similar linear dispersion characteristics, and have monotonically increasing effective acoustic velocities by the order of the peak. The temperature and strain dependences of the first-peak resonance frequency ν_1 (i.e. Brillouin frequency shift) are investigated to be 0.99 MHz/°C and 0.038 MHz/με, respectively. These results are similar to those in all-silica optical fibers, and do not show significant feasibility for discriminative sensing of strain and temperature. Additionally, the SBS acousto-optic overlapping efficiency is measured to be ~50% indicating a two-fold enhancement of the SBS threshold.

Acknowledgments

The experimental study was completed at The University of Tokyo. This work is supported by the "Grant-in-Aid for Scientific Research (S)" and the "Global Center of Excellence Program (G-COE)" from the Ministry of Education, Culture, Sports, Science and Technology, Japan. Weiwen Zou is partially supported by the National Natural Science Foundation of China (Grant No. 61007052), the International Cooperation Project from the Ministry of Science and Technology of China (Grant No. 2011FDA11780), and the "SMC Young Star" Scientist Program of Shanghai Jiao Tong University.

#160578 - $15.00 USD Received 3 Jan 2012; revised 2 Mar 2012; accepted 31 Mar 2012; published 30 Apr 2012